Molecular-dynamics simulation of the static pair-pair correlation function for classical fluids

B. E. Clements,* C. E. Campbell, and P. J. Samsel
Department of Physics and Astronomy, University of Minnesota, 116 Church Street SE, Minneapolis, Minnesota 55455

F. J. Pinski
Department of Physics, University of Cincinnati, Cincinnati, Ohio 45221
(Received 10 January 1991)

We have used a molecular-dynamics simulation to calculate the first seven nonzero Legendre coefficients, $Q^{(l)}(r,r')$, of the static pair-pair correlation function $Q(\mathbf{r},\mathbf{r}')$. The interaction potential was taken to be Lennard-Jones. The simulations were done at two different values of density and temperature, one coinciding with that of liquid argon near its triple point and the other with liquid argon at 181.0 K. $Q(\mathbf{r},\mathbf{r}')$ can be expressed in terms of two, three-, and four-body distribution functions. We use the Kirkwood superposition approximation to estimate the three-body contribution to $Q(\mathbf{r},\mathbf{r}')$. We argue that at low densities the three-body correlations are substantially more important than the four-body correlations. The three-body part of the $l=4$ and 6 coefficients emphasizes configurations composed of nearest-neighbor triplets with internal angles of approximately 90° and 60°, respectively. We find that the $l=6$ coefficient shows a dramatic increase in structure at elevated density. Furthermore, this coefficient exhibits nearly periodic oscillations in its off-diagonal structure. Directions for future work are given.

I. INTRODUCTION

It has long been realized that a proper description of structural and thermodynamic properties of dense fluids requires a knowledge of multiparticle correlations. Extensive analytic and numerical studies have been carried out for the three-body distribution functions [1]. However, an important class of correlations, those between multiple pairs of particles, have largely been ignored [2,3]. The static pair-pair correlation function $Q(\mathbf{r},\mathbf{r}')$ is related to the probability of finding a pair of particles separated by $\mathbf{r}$ while simultaneously finding a second pair, not necessarily distinct, separated by $\mathbf{r}'$. It is the purpose of this study to determine $Q(\mathbf{r},\mathbf{r}')$ using a molecular-dynamics (MD) simulation. Formal definitions of $Q(\mathbf{r},\mathbf{r}')$ are given in Sec. II.

The pair-pair correlation function contains useful information about fluid structure. The specification of vectors $\mathbf{r}$ and $\mathbf{r}'$ requires a knowledge of both interatomic separations and relative interatomic orientations. Much of Sec. III is devoted to a discussion on the structural information obtained from $Q(\mathbf{r},\mathbf{r}')$. The pair-pair correlation function is also needed to calculate many thermodynamic quantities. This is because the correlation between any two-body functions A_2 and B_2, which are formed from two-body additive functions, can be expressed [2] in terms of $Q(\mathbf{r},\mathbf{r}')$:

$$\langle A_2B_2\rangle-\langle A_2\rangle\langle B_2\rangle = \left[\frac{N\rho}{2}\right]^2\int d\mathbf{r}\,d\mathbf{r}'a_2(\mathbf{r})b_2(\mathbf{r}')Q(\mathbf{r},\mathbf{r}')\,, \quad (1)$$

where

$$A_2=\sum_{\substack{i,j\\ i<j}}a_2(\mathbf{r}_{ij}),\quad B_2=\sum_{\substack{i,j\\ i<j}}b_2(\mathbf{r}_{ij})\,,$$

and ρ is the number density. For a system with a fixed number of particles which is characterized by a pairwise additive potential $u(r)$, the constant volume heat capacity C_v is one such example [1,4]

$$C_v=\tfrac{3}{2}Nk_B+\frac{\beta}{T}\left[\frac{N\rho}{2}\right]^2\int d\mathbf{r}\,d\mathbf{r}'u(\mathbf{r})u(\mathbf{r}')Q(\mathbf{r},\mathbf{r}')\,. \quad (2)$$

A second term proportional to the isothermal compressibility, χ_T, must be added to Eq. (2) for systems with particle number fluctuations. However, near the triple point of a dense fluid, where $\rho\chi_T/\beta\approx 0.02$, this term is expected to be small [5,6].

The pair-pair correlation function is also important in the high-temperature perturbation theory (the λ expansion [6]) of Zwanzig [7]. In that theory one develops a series expansion for the configuration free energy A:

$$e^{-\beta A}=\frac{\Lambda^{-3N}}{N!}\int d(\mathbf{r}_1,\ldots,\mathbf{r}_N)e^{\beta V}\,, \quad (3)$$

where Λ is the thermal wavelength. V is two-body additive and consists of a reference (unperturbed) potential V_0 and a perturbation V_1:

$$V=V_0+V_1=\sum_{\substack{i,j\\ i<j}}v_0(r_{ij})+\sum_{\substack{i,j\\ i<j}}v_1(\mathbf{r}_{ij})\,. \quad (4)$$

Expanding the excess (perturbed) free energy $A-A_0$ in powers of β, one obtains

$$A = A_0 + \frac{N\rho}{2}\int d\mathbf{r}\, v_1(r) g_0(r) - \frac{\beta}{2}\left[\frac{N\rho}{2}\right]^2 \int d\mathbf{r}\, d\mathbf{r}' v_1(\mathbf{r}) v_1(\mathbf{r}') Q_0(\mathbf{r},\mathbf{r}') \cdots , \quad (5)$$

where the subscripts on the radial distribution function $g_0(r)$, and $Q_0(\mathbf{r},\mathbf{r}')$ refer to the reference system. Equation (5) is strictly true for systems with fixed particle number, but the comment following Eq. (2) is applicable here as well.

Our system consisted of 500 particles interacting through a Lennard-Jones potential. The interatomic interaction of liquid argon is known to be well represented by a Lennard-Jones 6-12 potential

$$V(r) = 4\varepsilon\left[\left[\frac{\sigma}{r}\right]^{12} - \left[\frac{\sigma}{r}\right]^{6}\right], \quad (6)$$

with the parameters $\sigma = 3.41$ Å and $\varepsilon/k_B = 119.8$ K and we shall occasionally refer to it in our discussions. The particles were confined to a cubical box with periodic boundary conditions. The MD simulation was done in the microcanonical ensemble, i.e., (N,V,E) held fixed. Two thermodynamic points were studied. The first point, hereafter referred to as (A), had an average reduced temperature T^* of 0.723 and a reduced density ρ^* of 0.834. For argon, this corresponds to a temperature of 86.6 K and a density of 1.41 g/cm^3 which is near its triple-point values [8] of 83.3 K and 1.435 g/cm^3. The second simulation, (B), was done at a slightly lower reduced density of 0.800 and an average T^* of 1.511. This corresponds to liquid argon at 181.0 K.

In our simulation the equation of motion was integrated 90 000 times using the Verlet algorithm [9]. The reason for the large number of configurations needed in the averaging is discussed below. In terms of liquid argon at phase point (A), the equations of motion were solved every 12.3 fs for a total time of approximately 1 ns. Since the dynamic properties are also interesting, and shall be reported at a later time, correlation function measurements were taken at every time step. The cutoff distance for the Lennard-Jones potential and the correlation function measurements were 2.5σ and $(\sigma/2)(N/\rho^*)^{1/3}$, respectively. For (A) this corresponds to a cutoff of approximately 4.2σ. The correlation functions were calculated by dividing the space spanning the 4.2σ into 120 radial bins.

The thermodynamic data, including the pressure, are given for (A) and (B) in Table I. We also include our values for the diffusion constants. In an MD simulation the most accurate method for obtaining the pressure is through the virial [6]. Rather than expending additional memory and CPU time, the pressures quoted in Table I were obtained directly from our MD determined $g(r)$:

$$\frac{p}{\rho k_B T} = 1 - \frac{2\pi\rho}{3k_B T}\int_0^\infty \frac{\partial V(r)}{\partial r} g(r) r^3 dr . \quad (7)$$

$g(r)$ was assumed to be exactly unity for r greater than the correlation function cutoff. Although the pressures in Table I agree reasonably well with those in the literature [8,10], it is important to note that the high-pressure value has a rather large uncertainty associated with it. This uncertainty is not due to the radial cutoff but rather to the finite bin width used in the $g(r)$ calculation. It was observed that shifting the $g(r)$ radial grid [relative to the $\partial V(r)/\partial r$ grid] by a fraction of a bin width could change the pressure by as much as 35%. The origin of this uncertainty is the increasing accessibility of the core region of the potential at high temperatures. Even a small radial shift in $g(r)$ can have a large influence on the pressure.

The diffusion constants were calculated by integrating our MD velocity autocorrelation function over time:

$$D = \frac{k_B T}{m}\int_0^\infty \frac{\langle \mathbf{v}(0)\cdot\mathbf{v}(t)\rangle}{\langle v^2\rangle} dt , \quad (8)$$

where m is the particle mass and $\mathbf{v}(t)$ is the total velocity at time t. These values for D are in good agreement with other reported values [8,11].

In Sec. II, we give the formal definitions for $Q(\mathbf{r},\mathbf{r}')$ and its Legendre coefficients. For the most part, we have adhered to the definitions of Ref. [2]. In Sec. III, we present and discuss the results of the MD simulation. We apply the Kirkwood superposition approximation (KSA) to determine an approximate representation of the three-body correlations. Using this we provide plausibility arguments to explain the structure observed in $Q(\mathbf{r},\mathbf{r}')$. In Sec. IV, we give conclusions and suggestions for future work.

II. STATIC AND NONSINGULAR PAIR-PAIR CORRELATION FUNCTIONS

We follow Pinski and Campbell [2,12] and define the pair-pair correlation function as

TABLE I. Reduced densities ρ^*, temperatures T^*, pressures p^*, and diffusion constants D^* for MD runs (A) and (B). Also included are the corresponding variables for argon where $\rho = \rho^*(1/\sigma^3)$, $T = T^*(\varepsilon/k_B)$, $p = p^*(\varepsilon/\sigma^3)$, $D = D^*(\varepsilon\sigma^2/m)^{1/2}$. See text for discussions of p and D.

Run	ρ^*	ρ (g/cm^3) argon	T^*	T (K) argon	p^*	p (atm) argon	D^*	D (10^{-5} cm^2/sec) argon
(A)	0.834	1.41	0.723	86.6	0.13	54	0.034	1.8
(B)	0.800	1.35	1.511	181.0	3.8	1500	0.101	5.4

$$Q(\mathbf{r},\mathbf{r}')=\frac{1}{(N\rho)^2}\sum_{\substack{i,j\\ i\neq j}}\sum_{\substack{k,l\\ k\neq l}}[\langle\delta(\mathbf{r}-\mathbf{r}_{ij})\delta(\mathbf{r}'-\mathbf{r}_{kl})\rangle-\langle\delta(\mathbf{r}-\mathbf{r}_{ij})\rangle\langle\delta(\mathbf{r}'-\mathbf{r}_{kl})\rangle] . \tag{9}$$

In this equation N is the number of particles and ρ is the number density. The brackets indicate the usual thermodynamic average. The summations are over particles which are located by position vectors $\mathbf{r}_i$. We consider translation invariant homogeneous fluids only.

$Q(\mathbf{r},\mathbf{r}')$ can be expressed in terms of n-body distribution functions [2]:

$$g_n(\mathbf{r}'_1,\ldots,\mathbf{r}'_n)=\frac{N!}{(N-n)!}\frac{1}{\rho^n}\langle\delta(\mathbf{r}_1-\mathbf{r}'_1)\cdots\delta(\mathbf{r}_n-\mathbf{r}'_n)\rangle . \tag{10}$$

The result is

$$NQ(\mathbf{r},\mathbf{r}')=\rho\int d\mathbf{R}[g_4(\mathbf{R},\mathbf{R}+\mathbf{r},\mathbf{r}',0)-g(\mathbf{r})g(\mathbf{r}')]+g_3(\mathbf{r},\mathbf{r}',0)+g_3(-\mathbf{r},\mathbf{r}',0)+g_3(\mathbf{r},-\mathbf{r}',0)$$
$$+g_3(-\mathbf{r},-\mathbf{r}',0)+\frac{g(r)}{\rho}[\delta(\mathbf{r}-\mathbf{r}')+\delta(\mathbf{r}+\mathbf{r}')] . \tag{11}$$

The four-body term results when all particle labels are different, $i\neq j\neq k\neq l$; the three-body terms arise from the different permutations, $i\neq j\neq k$ but $l=i$ or j or k; and the two-body term results from the cases where $i\neq j$, $k\neq l$ but $i=k$, $j=l$, or $i=l$, $j=k$. When we analyze the results of the MD simulation in Sec. III we will argue that much of the qualitative behavior of $Q(\mathbf{r},\mathbf{r}')$ is due to the three-body correlations and that the primary effect of the four-body correlations is to enhance or diminish this behavior. $Q(\mathbf{r},\mathbf{r}')$ can be rigorously decomposed into three- and four-body correlations:

$$NQ(\mathbf{r},\mathbf{r}')=\frac{g(r)}{\rho}[\delta(\mathbf{r}-\mathbf{r}')+\delta(\mathbf{r}+\mathbf{r}')]$$
$$+2T(\mathbf{r},\mathbf{r}')+2T(\mathbf{r},-\mathbf{r}')+Q_4(\mathbf{r},\mathbf{r}') , \tag{12}$$

where the triplet and quartic correlation functions are defined by

$$T(\mathbf{r},\mathbf{r}')=\frac{1}{N\rho^2}\sum_{\substack{i,j,k\\ i\neq j\neq k}}[\langle\delta(\mathbf{r}-\mathbf{r}_{ij})\delta(\mathbf{r}'-\mathbf{r}_{kj})\rangle$$
$$-\langle\delta(\mathbf{r}-\mathbf{r}_{ij})\rangle\langle\delta(\mathbf{r}'-\mathbf{r}_{kj})\rangle] \tag{13}$$

and

$$Q_4(\mathbf{r},\mathbf{r}')=\frac{1}{N\rho^2}\sum_{\substack{i,j,k,l\\ i\neq j\neq k\neq l}}[\langle\delta(\mathbf{r}-\mathbf{r}_{ij})\delta(\mathbf{r}'-\mathbf{r}_{kl})\rangle$$
$$-\langle\delta(\mathbf{r}-\mathbf{r}_{ij})\rangle\langle\delta(\mathbf{r}'-\mathbf{r}_{kl})\rangle] . \tag{14}$$

Using a cluster representation for the three- and four-body distribution functions it can be shown [13] that $Q(\mathbf{r},\mathbf{r}')$ is of order $1/N$. Consequently, the terms in Eq. (9) which are of order unity must cancel to order $1/N$. In turn this requires significantly more configurations to be averaged in an MD or Monte Carlo simulation than the distribution functions themselves, where convergence to such a high degree is not usually necessary.

From Eq. (12), we define a nonsingular pair-pair distribution function $H(\mathbf{r},\mathbf{r}')$:

$$H(\mathbf{r},\mathbf{r}')=NQ(\mathbf{r},\mathbf{r}')-\frac{g(r)}{\rho}[\delta(\mathbf{r}-\mathbf{r}')+\delta(\mathbf{r}+\mathbf{r}')] . \tag{15}$$

$H(\mathbf{r},\mathbf{r}')$ is of order unity and is well behaved when $\mathbf{r}=\pm\mathbf{r}'$. Furthermore, $H(\mathbf{r},\mathbf{r}')$ depends only on the three- and four-body distribution functions.

For an isotropic and homogeneous fluid $Q(\mathbf{r},\mathbf{r}')$ and $H(\mathbf{r},\mathbf{r}')$ are functions of radial separations r and r' and the angle θ subtending the vectors $\mathbf{r}$ and $\mathbf{r}'$ and consequently can be expanded in a Legendre series. Pinski and Campbell [2] have demonstrated that the expansion coefficients of the Legendre series (their Legendre projections) provide a convenient means for displaying the information contained in $Q(\mathbf{r},\mathbf{r}')$. Furthermore, the Legendre projections themselves appear in a number of applications such as depolarized light scattering [14] and dielectric constant studies [15]. In regards to the first point, the alternative is to calculate $Q(\mathbf{r},\mathbf{r}')$ for fixed $\mathbf{r}$ and $\mathbf{r}'$. This is the most common means of displaying the three-body correlation function. Typically one fixes one or two out of the three variables and displays by contour or linear plots the remaining two or one variables, respectively. In the present work, we calculate the Legendre projections because, although only a finite number of them can be calculated, all the information for a given projection can be displayed.

Formally, the Legendre projections $H^{(l)}(r,r')$ are defined through the completeness relation for the spherical harmonics:

$$H(\mathbf{r},\mathbf{r}')=\sum_{l=0}^{\infty}\sum_{m=-l}^{l}H^{(l)}(r,r')Y_{lm}(\Omega_r)Y^*_{lm}(\Omega_{r'}) , \tag{16}$$

where $(\Omega_r)=(\theta_r,\phi_r)$ and $(\Omega_{r'})=(\theta_{r'},\phi_{r'})$ refer to a space-fixed coordinate system. Equation (16) can easily be inverted [16] and the result is

$$H^{(l)}(r,\mathbf{r})=\frac{1}{N(\rho r r')^2}\left\langle\left[\sum_{\substack{i,j\\ i\neq j}}\delta(r-r_{ij})Y_{lm}(\Omega_{ij})\right]\left[\sum_{\substack{k,p\\ k\neq p}}\delta(r-r_{kp})Y^{*}_{lm}(\Omega_{kp})\right]\right\rangle$$
$$-4\pi N g(r)g(r')\delta_{l,0}-2\frac{g(r)}{\rho}\frac{\delta(r-r')}{r^2}\ , \tag{17}$$

where $g(r)$ is the radial distribution function

$$g(r)=\frac{1}{4\pi N\rho r^2}\left\langle\sum_{\substack{i,j\\ i\neq j}}\delta(r-r_{ij})\right\rangle\ . \tag{18}$$

Rotation invariance of an isotropic fluid implies that any $m\in\{-l,\ldots,l\}$ can be chosen. We investigated the possibility of a loss of rotation invariance in our MD simulation. We compared $H^{(l)}(r,r';m=0)$ and the arithmetic mean over the various m values for the first few l values. We found that averaging over m does not produce a quantitatively significant change. Similar conclusions are drawn in MD studies on depolarized light scattering which involve the $l=2$ projection [17,18]. Obviously, the odd l projections are identically zero.

III. RESULTS FROM THE MD SIMULATION

In this section we present the results from the MD simulation described in the Introduction. Although the two-body correlation function $h(r)=g(r)-1$ is well understood for the case of simple fluids, we briefly review those properties that are relevant to the present work. In Fig. 1, $h(r)$ is shown for (A) and (B). As is well known, the negative correlation at small radial separations is due to the short-range repulsive core in the Lennard-Jones potential. This is an excluded volume effect. Figure 1 indicates that (B) has less excluded volume than (A) which is consistent with the fact that as the temperature increases, more of the core region is accessible to neighboring atoms. The first positive peak is due to the nearest-neighbor atoms clustering around an atom due to the attractive part of the potential. We let $R_{\rm NN}$ denote the position of this peak. As indicated by the peak heights, (A) shows substantially more configurational order than (B).

Since this is the first time that an MD calculated pair-pair correlation function has been reported, a primary goal of this paper is to display as much structural detail as possible. Figures 2–15 are plots of $H^{(l)}(r,r')$ for $l=0$, 2, 4, 6, 8, 10, and 12. The axes in these figures are the r and r' radial separations scaled by the Lennard-Jones parameter σ. The contours and three-dimensional graphs have negligible structure for r and r' less than that shown in these plots. For clarity, we have suppressed the uniform background of fluctuations which we regard as statistical noise. The magnitude of these fluctuations never exceeds a few percent of the heights of the major peaks.

Much of the structure shown in these plots can be understood from simple energy and relative-atomic-orientation considerations. For a qualitative understanding, it suffices to consider a small number of particles while completely ignoring the full many-body effects and entropy considerations. From the rotation symmetries of a simple fluid, the spherical harmonic addition theorem implies that an alternative form for Eq. (17) is

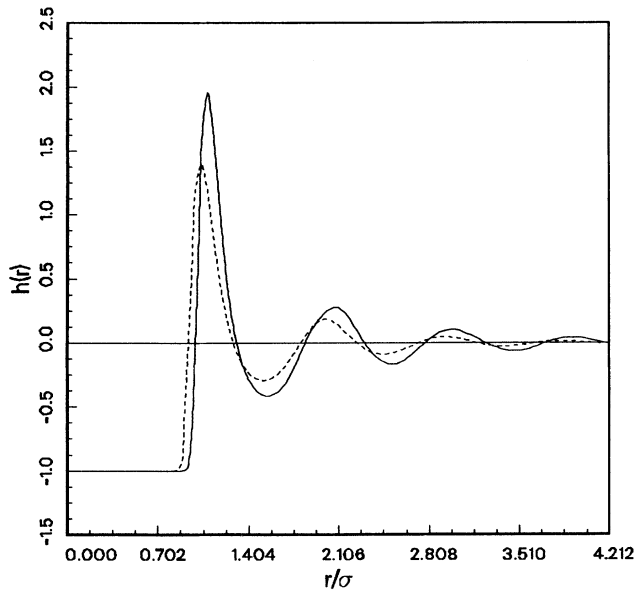

FIG. 1. $h(r)$ for (A) (solid) and (B) (dashed).

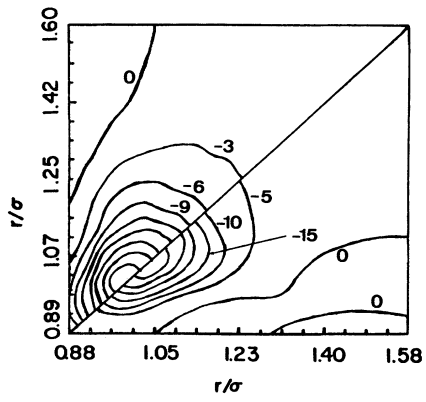

FIG. 2. Contours of MD $H^{(0)}(r,r')$ for (A) (bottom half) and (B) (top half). Contours near $r=r'=R_{\rm NN}$ continue with increments of -5 [-3] for (A) [(B)].

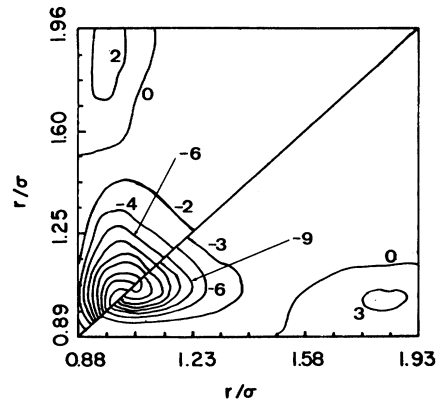

FIG. 3. Contours of MD $H^{(2)}(r,r')$ for (A) (bottom half) and (B) (top half). Contours near $r=r'=R_{\mathrm{NN}}$ continue with increments of -3 [-2] for (A) [(B)].

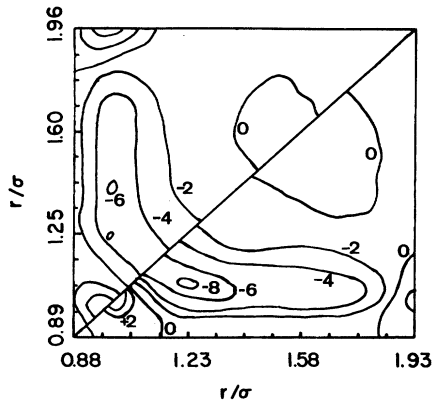

FIG. 4. Contours of MD $H^{(4)}(r,r')$ for (A) (bottom half) and (B) (top half).

$$H^{(l)}(r,r')=\frac{1}{4\pi N(\rho rr')^2}\sum_{\substack{i,j\\ i\neq j}}\sum_{\substack{k,p\\ k\neq p}}\langle\delta(r-r_{ij})\delta(r'-r_{kp})P_l(\cos\theta_{ij,kp})\rangle-4\pi Ng(r)g(r')\delta_{l,0}$$
$$-2\frac{g(r)}{\rho}\frac{\delta(r-r')}{r^2}\,, \tag{19}$$

where $\theta_{ij,kp}$ is the angle subtended by vectors $\mathbf{r}_{ij}$ and $\mathbf{r}_{kp}$. This observation is particularly useful since it allows one to consider the relative-interatomic orientations rather than angles measured from a space-fixed coordinate system.

Recall that since the self-term in Eq. (19) removes the two-body contribution, $H^{(l)}(r,r')$ is composed of only three- and four-body terms. To obtain an estimate of the importance of the three-body contribution we have used the Kirkwood superposition approximation to calculate the triplet correlation function $T^{(l)}(r,r')$:

$$T^{(l)}_{\mathrm{KSA}}(r,r')=g(r)g(r')[g^{(l)}(|\mathbf{r}-\mathbf{r}'|)-4\pi\delta_{l,0}]\,, \tag{20}$$

where

$$g^{(l)}(|\mathbf{r}-\mathbf{r}'|)=2\pi\int_{-1}^{1}d\omega\, g(r^2+r'^2-2rr'\omega)^{1/2}P_l(\omega)\,. \tag{21}$$

It follows from Eq. (12) that $H^{(l)}=4T^{(l)}+Q^{(l)}_4$. Using $g(r)$ obtained from (A) we have calculated $T^{(l)}_{\mathrm{KSA}}(r,r')$. Figure 16 is a plot of $4T^{(6)}_{\mathrm{KSA}}(r,r')$. This figure is to be compared with Fig. 11. One finds qualitative agreement between the two plots although $4T^{(6)}_{\mathrm{KSA}}(r,r')$ accounts for only half of the primary peak observed in Fig. 11. This difference has two origins; the absence of four-body correlations and the KSA. It is well known that the KSA

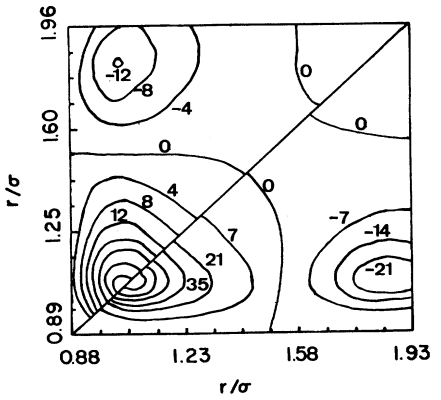

FIG. 5. Contours of MD $H^{(6)}(r,r')$ for (A) (bottom half) and (B) (top half). Contours near $r=r'=R_{\mathrm{NN}}$ continue with increments of 14 [4] for (A) [(B)].

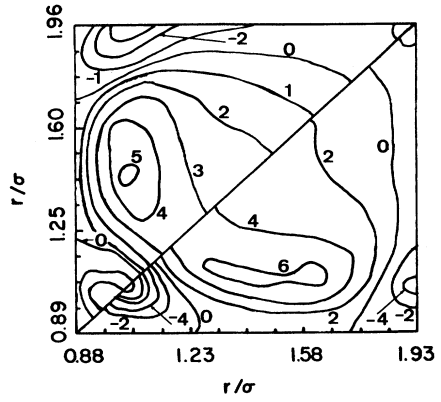

FIG. 6. Contours of MD $H^{(8)}(r,r')$ for (A) (bottom half) and (B) (top half).

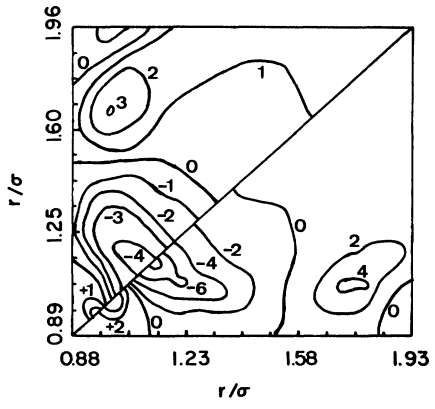

FIG. 7. Contours of MD $H^{(10)}(r,r')$ for (A) (bottom half) and (B) (top half). Contours near $r=r'=R_{NN}$ continue with increments of -2 for (A).

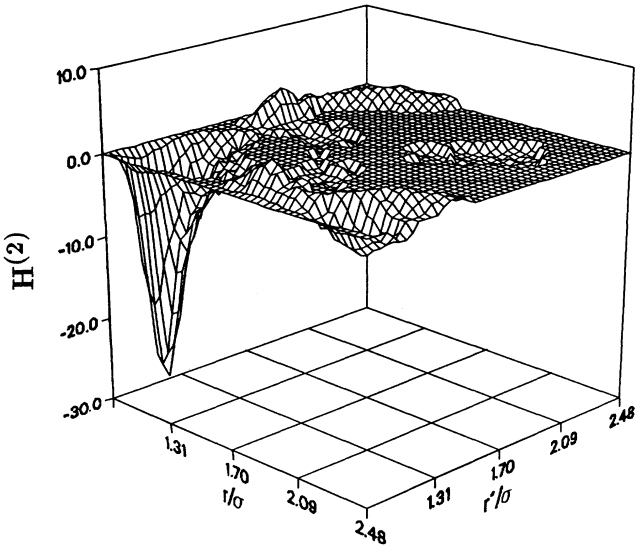

FIG. 9. Three-dimensional plot of MD $H^{(2)}(r,r')$ for (A).

works best at low densities and can provide only a qualitative description near the triple-point density. This is clear from $4T^{(6)}_{KSA}(r,r')$ calculated for (B). In that case the KSA accounts for 85% of the MD peak. Similar results are found for the other l projections. We conclude that three-body correlations are responsible for much of the qualitative structure of $H^{(l)}(r,r')$ at these densities although four-body correlations probably become increasingly important near the triple point. Given the importance of three-body correlations one may interpret Eq. (19) as a measure of the population of energetically favorable triplets. Each triplet is weighted by $P_l(\cos\theta_{ijk})$ where θ_{ijk} is an internal angle of the triplet (i,j,k). Similarly, the four-body contribution is a measure of the population of energetic and orientational favorable quartics (i,j,k,p). These points will become clear from the examples discussed below.

We now consider the individual projections. The importance of the relative atomic orientations is clearest for projections with l greater than 0. In Fig. 9 the MD projection $H^{(2)}(r,r')$ is displayed from (A). The origin of the large negative peak can be attributed to an excluded volume effect. The peak is located at $r=r'=R_{NN}$. In Fig. 17(a), we show an energetically favorable configuration of four atoms, which in a crystal would correspond to the beginnings of a close-packed structure. Let the angle subtending vectors **R** and **S** be denoted by θ_{RS} and let $R=S=R_{NN}$. P_2 gives a large positive weight to $\theta_{RS}\approx 0°$ and 180° and a small negative weight to the energetically favored $\theta_{RS}\approx 60°$. Since triplets with $\theta_{RS}\approx 0°$ are prohibited by excluded volume considerations the net contri-

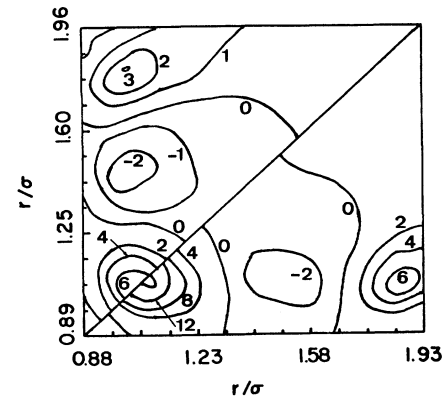

FIG. 8. Contours of MD $H^{(12)}(r,r')$ for (A) (bottom half) and (B) (top half). Contours near $r=r'=R_{NN}$ continue with increments of 4 for (A).

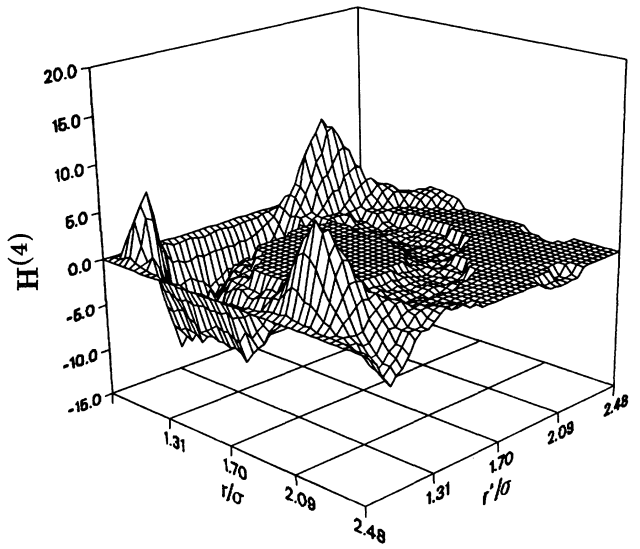

FIG. 10. Three-dimensional plot of MD $H^{(4)}(r,r')$ for (A).

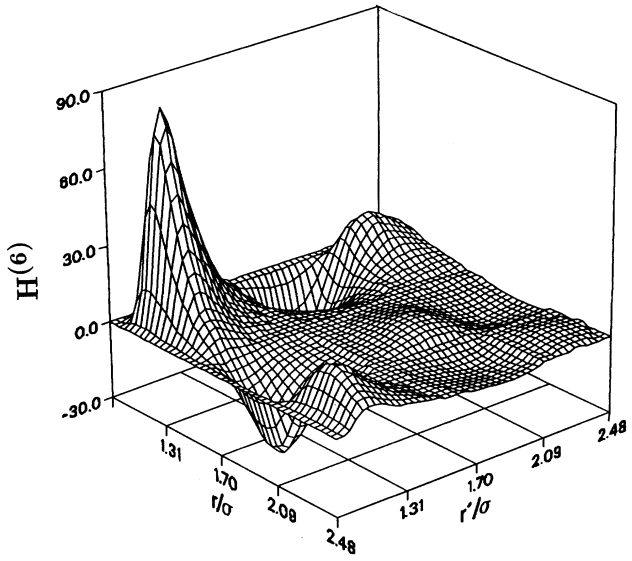

FIG. 11. Three-dimensional plot of MD $H^{(6)}(r,r')$ for (A).

bution from three-body correlations is expected to be negative at $r=r'=R_{NN}$. This argument obviously ignores contributions from less energetically favorable triplets such as $R=S=R_{NN}$ and $\theta_{RS}\approx 180°$. When considering the four-body contributions, nonplanar as well as planar arrangements of four particles are important. An energetically favored nonplanar arrangement is the tetrahedron shown in Fig. 17(a). In that case the angle subtended by vectors **R** and **T** is 90°. Consequently, this quartic contributes negatively to the total $Q_4^{(2)}(R_{NN},R_{NN})$. Although slightly less energetically

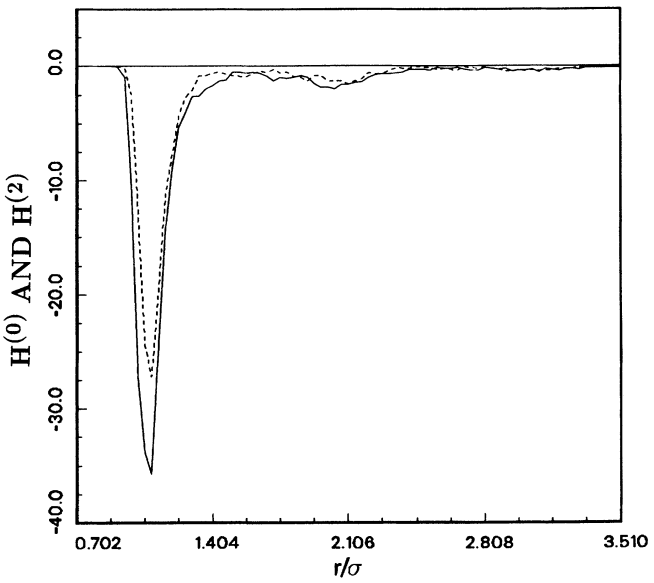

FIG. 12. MD $H^{(0)}(r,r)$ (solid) and $H^{(2)}(r,r)$ (dashed) as a function of r for (A).

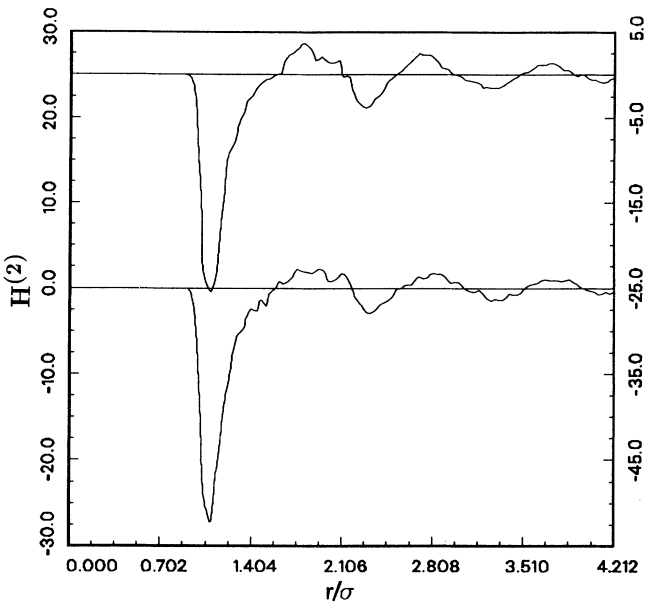

FIG. 13. Off-diagonal cuts of the MD $H^{(2)}(r,r')$ for (A). The left-vertical (right-vertical) scale corresponds to the lower (upper) curve. The lower curve is $H^{(2)}(r,r'=R_{NN})$ as a function of r. The upper curve is the same but r' shifted one bin width inward from R_{NN}. It is clear that the off-diagonal peaks do not take on their maximum values right at $r'=R_{NN}$.

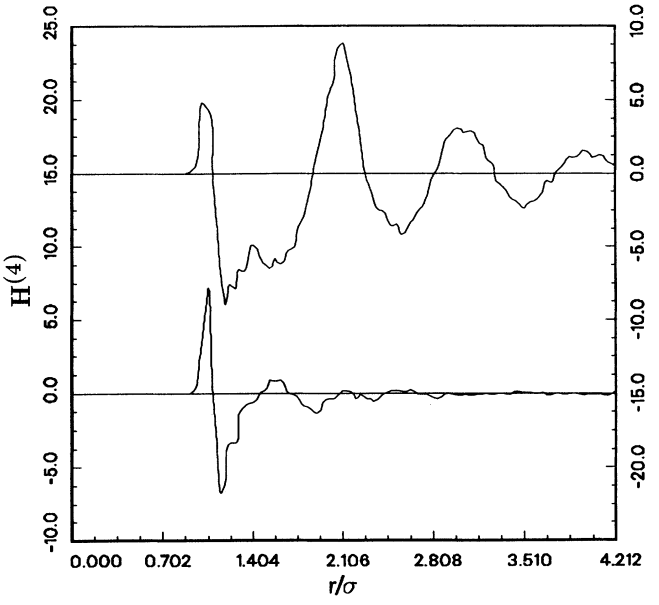

FIG. 14. Diagonal and off-diagonal cuts of the MD $H^{(4)}(r,r')$ for (A). The left-vertical (right-vertical) scale corresponds to the lower (upper) curve. The lower curve is $H^{(4)}(r,r)$ as a function of r. The upper curve is $H^{(4)}(r,r'=R_{NN})$ as a function of r.

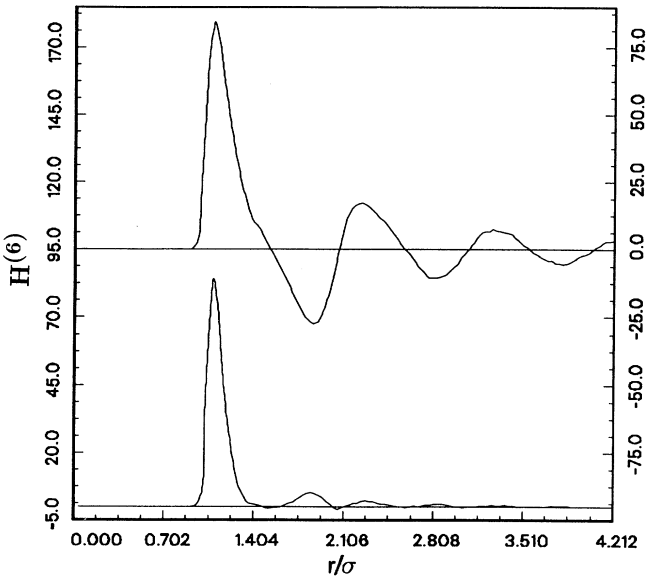

FIG. 15. Same as Fig. 14 but for $H^{(6)}(r,r')$.

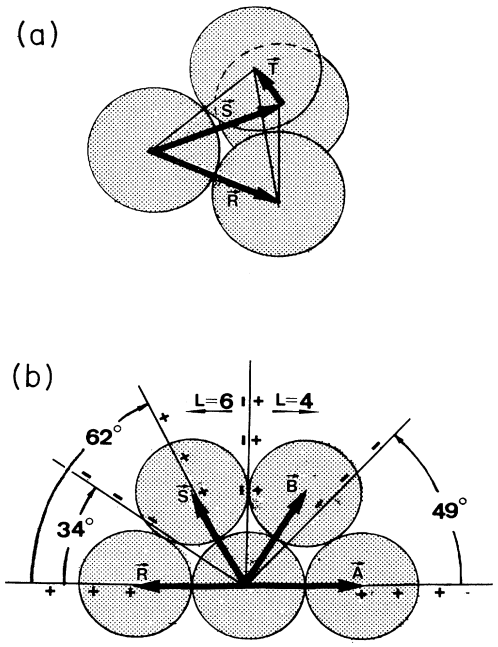

FIG. 17. (a) Energetically favorable arrangement of four atoms interacting by a Lennard-Jones potential. (b) Energetically favorable arrangements of three atoms and the positions of maximal positive and negative weights from P_4 (right of the vertical line) and P_6 (left of the vertical line).

favorable, there exists planar quartics which have orientation weights of $+1$, independent of l. These quartics correspond to shifting the fourth member of the tetrahedron [Fig. 17(a)] in the RS plane such that close packing is maintained. The vectors **R** and **T** are then parallel or antiparallel. For this reason there is probably a substantial cancellation of four-body terms in projections which give negative weight to angles of approximately 90°. These are the $l=2$, 6, and 10 projections.

From Fig. 9 it is also apparent that $H^{(2)}(r,r')$ has off-diagonal ($r\neq r'$) structure. Positive peaks are observed in the neighborhood of $r\approx R_{\mathrm{NN}}$ and $r'\approx 2R_{\mathrm{NN}}$ (and its reflection about $r=r'$). This structure is best displayed in Fig. 13. The origin of this structure can be at least partially attributed to the triplet formed when $\theta_{RS}\approx 180°$. In that case one side of the triangle is approximately $2R_{\mathrm{NN}}$. Finally, we note that $T^{(2)}_{\mathrm{KSA}}(r,r')$ also exhibits off-diagonal structure, although substantially exceeding the MD value.

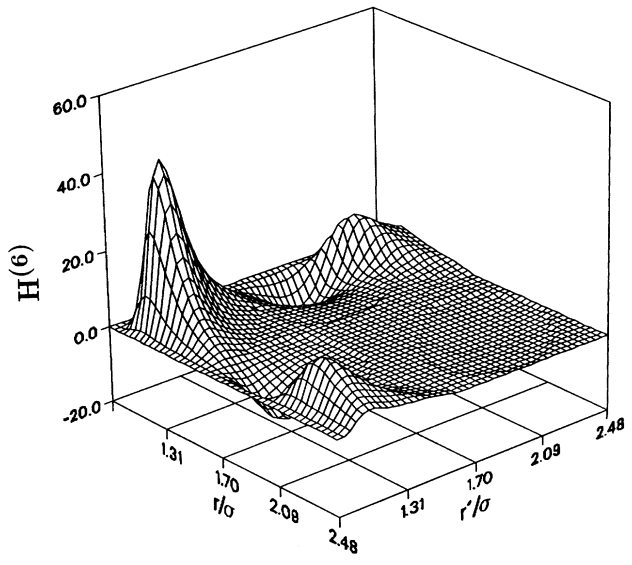

FIG. 16. Three-dimensional plot of $4T^{(6)}_{\mathrm{KSA}}(r,r')$ using the MD $g(r)$ from (A).

Returning to $H^{(0)}(r,r')$ one again finds a large negative peak at $r=r'=R_{\mathrm{NN}}$ (see Figs. 2 and 12). In this case the negative correlation must come from the subtracted $g(r)g(r')$ term in Eq. (19). From Fig. 2 it can be seen that the off-diagonal structure, that was observed in $H^{(2)}(r,r')$, is much less significant in this case. This supports the explanation that the off-diagonal structure in $H^{(2)}(r,r')$ is due to P_2.

The diversity of structure contained in $H^{(l)}(r,r')$ is exemplified by the $l=4$ and 6 projections. These cases are shown in Figs. 4, 5, 10, 11, 14, and 15. In Fig. 17(b) we show the energetically favored triplet configuration. To the right (left) of the vertical line we show the angles corresponding to the extreme values of P_4 (P_6). For example, P_4 acquires its most negative value at approximately 49°. It is immediately clear that one expects a large positive three-body contribution to $H^{(6)}(R_{\mathrm{NN}},R_{\mathrm{NN}})$ from this configuration. Furthermore, a nearly frozen liquid which favors close packing would have a very large population of these triplets. In the $l=4$ case we see that the energetically favored configuration has a negative

weight from P_4. However, the triplet described by $\theta_{AB} \approx 90°$ should be expected to contribute significant positive weight to the total three-body contribution. The issue is further complicated by the addition of four-body contributions. From our previous discussion, we expect a positive contribution from $Q_4^{(4)}(R_{\rm NN}, R_{\rm NN})$. Consequently, one might expect a fair degree of "cancellation" in $H^{(4)}(r,r')$. In fact, relative to the other low l projections, $H^{(4)}(r,r')$ has small peaks and shallow valleys which is evidence for large cancellation in correlations.

Continuing in this way, the structure observed in the remaining figures can (at least partially) be explained. The analysis becomes less clear with increasing l, however,

We close this section with a discussion of the density and temperature dependence of the $H^{(l)}(r,r')$. The contours in Figs. 2–8 correspond to state points (A) and (B). All projections show an increase in structure with decreasing temperature and increasing density. Of particular interest is the rather dramatic increase in structure of $H^{(6)}(r,r')$ at $r=r'=R_{NN}$ as the thermodynamic state changes from (B) to (A). Furthermore, from Fig. 15 it is clear that the off-diagonal peaks of $H^{(6)}(r=R_{\rm NN},r')$ oscillate nearly periodically. These oscillations occur at $r'=R_{\rm NN}, 2R_{\rm NN}, \ldots$. These observations are very suggestive that the prevailing crystalline structure is likely to be close packed for this system. Parenthetically, liquid argon is known to freeze into a (close-packed) fcc crystal.

IV. CONCLUSIONS

Using MD we have calculated the Legendre coefficients of the static pair-pair correlation function. Our simulation was done with N, V, and E held fixed. For completeness we mention that Lebowitz, Percus, and Verlet [19] and Wallace and Straub [20] have discussed how one extends MD ensemble calculations to canonical ensembles.

We have demonstrated how the static pair-pair correlation function can yield new information about fluid structure. We used the KSA as an indicator of the importance of the three-body correlations in $H(\mathbf{r},\mathbf{r}')$. Clearly, this must be considered as a first step and an MD determined $T(\mathbf{r},\mathbf{r}')$ is necessary for the arguments proposed in this work to be made rigorous.

It would be interesting to examine the role of the interatomic potential in determining the behavior of the pair-pair correlation function. The pair-pair correlation function for a Lennard-Jones liquid provides a strong indication that the solid phase crystal structure will be close packed. One could calculate the pair-pair correlation function for a system, such as a liquid metal, that is known to freeze into a bcc crystal structure. This would deepen our understanding of the pair-pair correlation function as well as reveal its usefulness for discriminating different interatomic potentials.

We presently have work underway in the following directions. First, we are using the MD determined pair-pair correlation function to assess the quality of the integral equation of Pinski and Campbell [2]. The Pinski-Campbell integral equation provides an analytic means for calculating $H(\mathbf{r},\mathbf{r}')$ and is based on the hypernetted chain (HNC/0) approximation. Although this approximation is expected to fail at high densities, it should produce quantitatively accurate results at lower densities. From the standpoint that the Pinski-Campbell $H(\mathbf{r},\mathbf{r}')$ is much more economical to generate than the MD $H(\mathbf{r},\mathbf{r}')$, it is very important to have a quantitative measure of its accuracy. Secondly, we have also calculated the dynamic pair-pair correlation function $H(\mathbf{r},\mathbf{r}';t)$ and those results are planned to be reported in a subsequent paper.

ACKNOWLEDGMENTS

Support from the University of Minnesota Supercomputer Institute, the National Science Foundation under Contract No. PHY-8806265, and Texas Advanced Research Program under Grant No. 010366-012 is gratefully acknowledged.

*Present address: Center for Theoretical Physics, Texas A&M University, College Station, TX 77843.

[1] H. J. Raveché and R. D. Mountain, in *Progress in Liquid Physics,* edited by C. A. Croxton (Wiley, New York, 1978), p. 469 and references therein.
[2] F. J. Pinski and C. E. Campbell, Phys. Rev. A **33**, 4232 (1986).
[3] J. Blawzdziewicz, B. Cichocki, and G. Szamel, J. Chem. Phys. **91**, 7467 (1989).
[4] P. Schofield, Proc. Phys. Soc. **88**, 149 (1966).
[5] L. Verlet, Phys. Rev. **165**, 201 (1968).
[6] J. P. Hansen and I. R. McDonald, *Theory of Simple Fluids* (Academic, New York, 1976).
[7] R. Zwanzig, J. Chem. Phys. **22**, 1420 (1954).
[8] D. Levesque, L. Verlet, and J. Kürkijarvi, Phys. Rev. A **7**, 1690 (1973).
[9] L. Verlet, Phys. Rev. **159**, 98 (1967).
[10] J. A. Barker and D. Henderson, J. Chem. Phys. **47**, 4714 (1967) (Fig. 5).
[11] J. Naghizadeh and S. A. Rice, J. Chem. Phys. **36**, 2710 (1962); P. Borgelt, C. Hoheisel, and G. Stell, Phys. Rev. A **42**, 789 (1990).
[12] Our static pair-pair correlation function $Q(\mathbf{r},\mathbf{r}')$ is denoted by $P_{2,2}(\mathbf{r},\mathbf{r}')$ in Ref. 2.
[13] The proof follows from arguments found in E. Feenberg, *Theory of Quantum Fluids* (Academic, New York, 1969), Chap. 2.
[14] F. J. Pinski and C. E. Campbell, Chem. Phys. Lett. **56**, 156 (1978).
[15] P. Mazur and U. Geigenmuler, Physica A **136**, 316 (1986).
[16] See also C. E. Campbell and F. J. Pinski, Nucl. Phys. **A328**, 210 (1979).
[17] B. J. Adler, J. J. Weis, and H. L. Strauss, Phys. Rev. A **7**, 281 (1973).
[18] U. Balucani and R. Vallauri, Mol. Phys. **38**, 1099 (1979).
[19] J. L. Lebowitz, J. K. Percus, and L. Verlet, Phys. Rev. **153**, 250 (1967).
[20] D. C. Wallace and G. K. Straub, Phys. Rev. A **27**, 2201 (1983).